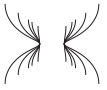
JGSP **54** (2019) 55–78

JOURNAL OF
Geometry and Symmetry in Physics
ISSN 1312-5192

ROTATING LIQUID DROPS AND DELAUNAY SURFACES

VLADIMIR I. PULOV AND IVAÏLO M. MLADENOV

Presented by Ivaïlo M. Mladenov

Abstract. Here we consider the problem of finding the equilibrium configurations of a rotating liquid drop, paying special attention to the cases when the droplet takes the shape of a Delaunay surface. By making use of the canonical forms of the elliptic integrals and the Jacobian elliptic functions we have derived several explicit parameterizations of the Delaunay surfaces. They are expressed relying on two independent real parameters accounting respectively the size and the shape so that all possible Delaunay surfaces are represented in a unified way.

MSC: 53A04, 53A05, 53A10, 53B50, 33E05, 76B45, 76D45
Keywords: Axially symmetric surfaces, capillarity, curves, elliptic integrals, fluid dynamics, Jacobian elliptic functions, parameterizations, surface geometry

Contents

1. Introduction

This paper is a continuation of our previous work [20], where we have considered the problem about the shape of the rotating liquid drop in the special case with a

hidden parameter, meaning that one of the integration constants has been set to zero (cf. also [12]). Here we proceed in a similar fashion with another interesting case in which the droplets have the shapes of the Delaunay surfaces. Our principal goal in all of the considered cases, here and in the aforementioned paper [20], remains the same – finding the explicit parameterizations of all possible shapes of the rotating liquid drops (recall, there does not exist elementary functions representation of these surfaces) and classifying them in an unified and purely geometrical way. As in the preceding paper [20], we are going to make use of the Jacobian elliptic functions and the elliptic integrals (cf. Section 3). Let us mention that in [12] these surfaces were considered in terms of the Weierstrassian functions.

In many references the surfaces we are interested in are called *capillary surfaces*. Such surfaces represent the interfaces arising between two immiscible fluids. The shape of the capillary surface in fluid statics is determined by balancing the surface tension σ and the pressure difference p exerted on the opposite sides of the interface according to the *Laplace-Young equation*

$$p = \sigma H \tag{1}$$

in which H is the mean (meaning average) curvature of the capillary surface. The Laplace-Young equation was introduced around 1800 by Thomas Young and Pierre-Simon Laplace to explain the existence of "curved" capillary surfaces, such as menisci, soap bubbles, liquid drops, etc. (about soap films, cf. [14]).

It was in 1850s when the Belgian mathematician and physicist Joseph Plateau launched his famous experiments with rotating liquid drops. He observed that under the radial action of the centrifugal force, the initially spherical liquid drops deform continuously to take, according to their angular velocity, different axisymmetric shapes [18]. The first rigorous description of these shapes was given in Lord Rayleigh's paper [22]. He showed that the shape of the drop depends on the *rotation rate parameter*, which in our notation (see the equation (4) below) is given by $\tilde{a}r^3$. Since then many authors have explored the rotation rate parameter in their study of both the shape and the stability of the rotating liquid drops (see, e.g., [3, 5, 12, 13]). In a more general sense cylindrical [16, 21] and non-axisymmetric configurations [8] have been also considered.

In our work on Plateau's rotating liquid drops, instead of using the rotation rate parameter or any other parameters that are "physical in nature", we prefer to introduce parameters of pure geometrical character (like the couple r and ν defined in the next Section 2) which allow us to present several explicit parameterizations of the drop's possible shapes and to classify them in a transparent geometrical manner (see reference [20], Section 4 and Section 5 of the present paper).

The first analytical (integral) representation and classification of the surfaces of revolution with constant mean curvatures (CMC *surfaces of revolution*) in the Euclidian space $\mathbb{R}^3$ was given in 1841 by the French astronomer and mathematician Charles-Eugène Delaunay [4]. Except planes, cylinders and spheres the complete list of such surfaces include catenoids, unduloids and nodoids, all of which are now called *Delaunay surfaces*. In the Appendix to the Delaunay's paper Sturm has presented another geometrical/mechanical description of the CMC surfaces of revolution by characterizing them variationally (see also [1]) and as surfaces generated by Delaunay roulettes, which are traces of the foci of the conic sections when these conics roll without slipping in a plane along the axis of revolution (Fig. 1). As it is well known Delaunay surfaces, unduloids and nodoids, are not expressible by elementary functions. Their alternative representations via special functions can be found in [6, 9, 10, 19]. In some broader sense the Delaunay surfaces are identified as rotational linear Weingarten surfaces obtained by binormal evolution of planar p-elastic curves, being in this case the Delaunay roulettes [17].

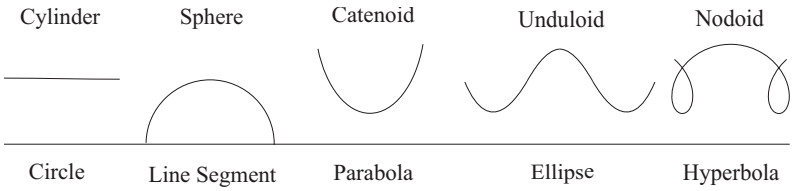

Figure 1. Delaunay roulettes (the profile curves of the Delaunay surfaces) generated by rolling the conics listed below them.

We are going to reveal that there exists an interesting connection between the Plateau's rotating liquid drops and the Delaunay's surfaces, namely, we will show that the Delaunay surfaces can also appear as particular shapes of rotating liquid drops.

After formulating the problem (Section 2) and giving some basic facts about the elliptic integrals and the Jacobian elliptic functions (Section 3), in the next two Sections 4 and 5, we establish four specific classes of Delaunay shapes (portions of unduloids and nodoids) formed by the rotating liquid drop, presenting three alternative explicit parameterizations for the surfaces of each of these classes.

2. Formulation of the Problem

In our further considerations we assume that a drop of an incompressible liquid, immiscible with another fluid in which it is immersed, is revolved with constant

velocity ω about some "vertical" fixed axis OZ. We assume also that the action of gravity has been excluded. Then the drop is held together within a finite enclosing surface $\mathcal{S}$ only by the surface tension σ, and the equilibrium of its shape is attained if the resulting pressure at every point of $\mathcal{S}$, being the boundary with the ambient fluid, disappears. The pressure at the interface of the two mediums arise from three causes, the external p_e and internal p_i pressures to which the respective liquids outside and inside of the drop are subjected, the capillary pressure σH, proportional to the mean curvature H of the surface $\mathcal{S}$ according to the Laplace-Young equation [11, 15], and the pressure $\dfrac{\rho\omega^2\mathcal{R}^2}{2}$ due to the centrifugal force acting at radial distance $\mathcal{R}$ from the axis of revolution and opposing the surface tension; ρ is the difference between the mass densities ρ_i of the inner and ρ_e of the exterior fluids. By balancing of all these pressures

$$p_i + \frac{\rho\omega^2\mathcal{R}^2}{2} = \sigma H + p_e \tag{2}$$

it can be immediately deduced that the mean curvature of the equilibrium shapes of the rotating liquid drop have the form

$$H = 2\tilde{a}\mathcal{R}^2 + \tilde{c} \tag{3}$$

where

$$\tilde{a} = \frac{\rho\omega^2}{4\sigma}, \qquad \tilde{c} = \frac{p}{\sigma}. \tag{4}$$

Note that $\tilde{a}$ and $\tilde{c}$ are arbitrary real constants, depending on the values of the physical parameters ω, σ, and the differences ρ and p of the respective mass densities and pressures in the vicinity of the two sides of $\mathcal{S}$

$$\rho = \rho_i - \rho_e, \qquad p = p_i - p_e. \tag{5}$$

As can be seen from equations (3) – (5), when the two fluids have equal mass densities, $\rho_i \equiv \rho_e$, the physical quantity $\tilde{a}$ equals to zero and the rotating liquid drop assumes CMC shapes of revolution with

$$H = \tilde{c}, \qquad \tilde{c} = \text{const}. \tag{6}$$

From now on the equilibrium shapes of the rotating liquid drop that we are going to deal with will be Delaunay surfaces which mean curvature is given by equation (6). For the the case of $\tilde{a} \neq 0$ the reader is referred to the papers [12, 20], where other possible axisymmetric shapes are presented and parameterized explicitly via

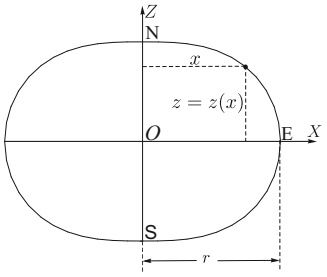

Figure 2. A typical closed profile curve in XOZ-plane.

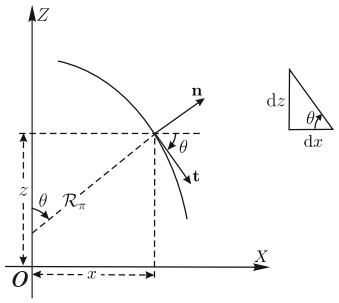

Figure 3. Geometry of the profile curve ($\mathcal{R}_\pi$ – parallel principal curvature).

Weierstrassian functions [12] or Jacobian elliptic functions and elliptic integrals [20].

Let the surface $\mathcal{S}$ under consideration, which is the surface of the drop itself, is generated by revolving (about the "vertical" axis OZ) the meridional section γ of $\mathcal{S}$, a curve lying in the XOZ-plane of an orthogonal coordinate system (OX, OY, OZ) in $\mathbb{R}^3$. Let this curve γ, which is the *profile curve* of $\mathcal{S}$, intersects the OX-axis at right angle and the function $z = z(x)$ specifying it for $x \geq 0$ is chosen in such a way that $z(r) = 0$, $r > 0$ (see Fig. 2). Then the curve on the surface traced by the point $(r, 0)$ of the profile curve is the *equator* of $\mathcal{S}$, which we assume to be with a predetermined (fixed) radius r.

By making use of the wellknown in classical differential geometry [15] relations between the mean curvature H, the meridional κ_μ and the parallel κ_π curvatures of $\mathcal{S}$, i.e.,

$$\kappa_\mu = \frac{\mathrm{d}(x\kappa_\pi)}{\mathrm{d}x}, \qquad H = \frac{\kappa_\mu + \kappa_\pi}{2} \tag{7}$$

it is straightforward to obtain for the considered CMC surfaces of revolution with $H = \tilde{c}$ (cf. equation (6)) the solutions

$$\kappa_\pi = \tilde{c} + \frac{m}{x^2}, \qquad \kappa_\mu = \tilde{c} - \frac{m}{x^2}. \tag{8}$$

where $m \in \mathbb{R}$ is an integration constant. As it can be inferred from simple geometrical considerations (cf. Fig. 3) and the relation $\kappa_\pi = 1/\mathcal{R}_\pi$, the profile curve $\gamma = (x, z(x))$ of the rotating liquid drop can be obtained by integrating the equation

$$\frac{\mathrm{d}z}{\mathrm{d}x} = \pm\frac{x\kappa_\pi}{\sqrt{1 - (x\kappa_\pi)^2}}. \tag{9}$$

In view of future applications, from now on, we will abandon the use of physical parameters, replacing $\tilde{c}$ and m by other two parameters having direct geometrical meaning.

We define

$$\nu = \frac{\mathring{\kappa}_\mu}{\mathring{\kappa}_\pi} = r\,\mathring{\kappa}_\mu \tag{10}$$

where $\mathring{\kappa}_\pi = 1/r$ and $\mathring{\kappa}_\mu$ are the parallel and the meridional principal curvatures evaluated along the equator E, i.e., for $\theta \equiv \mathring{\theta} = \pi/2$ (cf. Fig. 2 – Fig. 3 and the assumptions made above). In this setting the mean curvature of the droplet's surface at the points of the equator $\mathring{H} = (\mathring{\kappa}_\mu + \mathring{\kappa}_\pi)/2$ and equations (6), (8) and (10) produce the relations

$$\tilde{c} = \frac{1+\nu}{2r}, \qquad m = \frac{(1-\nu)r}{2}. \tag{11}$$

As a result the initially given constants $\tilde{c}$ and m have been expressed by the real parameters, $\nu \in \mathbb{R}$ and $r > 0$, which geometrical significance can be seen at once – the dimensionless quantity ν accounts for the type of the Delaunay surfaces, while the "length parameter" r controls their size. Three particular types of surfaces are easily recognized as right circular cylinders for $\nu = 0$, spheres for $\nu = 1$ and catenoids for $\nu = -1$.

Now, by substituting in the equation (9) the expression for κ_π from (8) and passing to the parameters ν and r by (11), the profile curve of the rotating liquid drop (its upper right branch) takes the form ($\nu \neq 0$)

$$z(\chi) = \pm\,\frac{r}{2}\int_\chi^1 \frac{((\nu+1)t - \nu + 1)\mathrm{d}t}{\sqrt{t(1-t)\,((\nu+1)^2 t - (\nu-1)^2)}}, \qquad \chi = \frac{x^2}{r^2} \tag{12}$$

in which for the surfaces lying inside the cylinder $\nu = 0$

$$x \in [0, r], \qquad \chi \in [0, 1], \qquad t \in (0, 1) \tag{13}$$

and for the surfaces positioned outside the cylinder

$$x \in [r, +\infty), \qquad \chi \in [1, +\infty), \qquad t \in (1, +\infty). \tag{14}$$

For two specific values of ν the above integral can be immediately evaluated to obtain (using only elementary functions) the sphere with $H = 1/r$ for $\nu = 1$ and the catenoid with $H = 0$ for $\nu = -1$ which profile curve, the catenary, is given by

$$z(x) = r\,\mathrm{arcsinh}\sqrt{\left(\frac{x}{r}\right)^2 - 1}, \qquad x \in [r, +\infty). \tag{15}$$

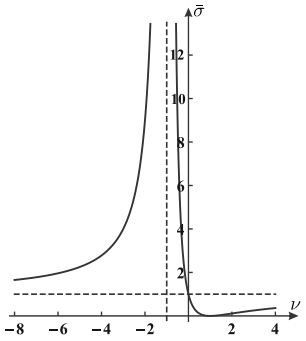

Figure 4. Graphic of the root $\bar{\sigma}$ versus ν (dashed lines are the asymptotes of the function).

The polynomial under the radical in (12) has three roots (for $\nu \neq -1$) all of which are real numbers

$$0, \qquad 1, \qquad \bar{\sigma} = \left(\frac{1-\nu}{1+\nu}\right)^2. \tag{16}$$

For the classification of the Delaunay shapes of the rotating liquid drop we need to know in what order these three roots are related to each other for each value of ν.

Based on the ranges of the root $\bar{\sigma}$ (cf. Fig. 4) and the possible types of Delaunay surfaces we can distinguish four particular classes of the drop's shapes (Fig. 5)

$$\begin{array}{lll} \mathcal{D}^{\mathrm{I}}(\nu) & \nu \in (-\infty, -1) & 0 < 1 < \sigma_1 \\ \mathcal{D}^{\mathrm{II}}(\nu) & \nu \in (-1, 0) & 0 < 1 < \sigma_2 \\ \mathcal{D}^{\mathrm{III}}(\nu) & \nu \in (0, 1) & 0 < \sigma_3 < 1 \\ \mathcal{D}^{\mathrm{IV}}(\nu) & \nu \in (1, +\infty) & 0 < \sigma_4 < 1 \end{array} \tag{17}$$

where σ_i is the root $\bar{\sigma}$ ($\sigma_i \equiv \bar{\sigma}$) referred to the surfaces of the i-th class. Each one of the above classes consists of certain portions of Delaunay surfaces being, either

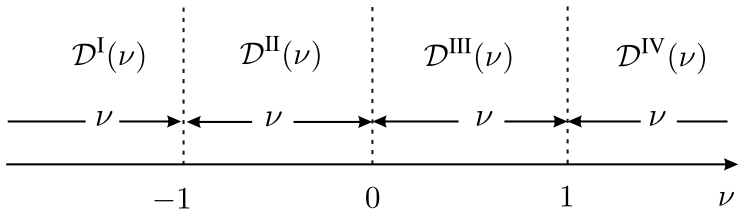

Figure 5. Ranges of the parameter ν related to different classes of shapes of the rotating liquid drop.

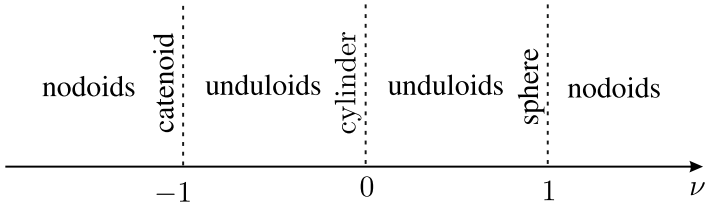

Figure 6. Ranges of the parameter ν related to different types of Delaunay surfaces.

nodoids of classes $\mathcal{D}^{\mathrm{I}}(\nu)$ and $\mathcal{D}^{\mathrm{IV}}(\nu)$, or unduloids of classes $\mathcal{D}^{\mathrm{II}}(\nu)$ and $\mathcal{D}^{\mathrm{III}}(\nu)$ (cf. Fig. 6 and the graphics of the profile curves in the next sections). The catenoid $\nu = -1$ and the surfaces $\mathcal{D}^{\mathrm{I}}(\nu)$ and $\mathcal{D}^{\mathrm{II}}(\nu)$ are lying outside the cylinder $\nu = 0$, while the sphere $\nu = 1$ and the other two classes of surfaces $\mathcal{D}^{\mathrm{III}}(\nu)$ and $\mathcal{D}^{\mathrm{IV}}(\nu)$ are positioned inside the cylinder.

For $\nu \neq 0, \pm 1$ the integral (12) belongs to the class of the so called *elliptic integrals*. Elliptic integrals do not have closed form representation in elementary functions. Our present goal is to build up the canonical forms of the elliptic integral (12) for all values of the parameter ν.

3. Elliptic Integrals and Jacobian Elliptic Functions

In the next sections we use the *normal elliptic integrals* of the first

$$F(\varphi, k) \equiv \int_0^{\zeta} \frac{\mathrm{d}t}{\sqrt{(1-t^2)(1-k^2t^2)}} = \int_0^{\varphi} \frac{\mathrm{d}\theta}{\sqrt{1-k^2\sin^2\theta}} \tag{18}$$

and the second kind

$$E(\varphi, k) \equiv \int_0^{\zeta} \sqrt{\frac{1-k^2t^2}{1-t^2}}\mathrm{d}t = \int_0^{\varphi} \sqrt{1-k^2\sin^2\theta}\,\mathrm{d}\theta. \tag{19}$$

These two fundamental elliptic integrals depend on the variable upper limit ζ or φ, which is considered as their *argument*

$$\zeta = \sin\varphi, \qquad \zeta \in (0, 1], \qquad \varphi \in (0, \frac{\pi}{2}]$$

and the so called *elliptic modulus* $k \in (0,1)$. There is only one more normal elliptic integral of third kind, which is not presented here as it is not needed for our considerations (for more details about the elliptic integrals and their normal forms, cf. [2]).

In order to reduce the elliptic integral (12) to its canonical form we will make substitutions involving *Jacobian elliptic functions* defined by the inversion of the elliptic integral of the first kind $u = F(\varphi, k)$. The new functions obtained by the inversion are called am (*amplitude*) and respectively sn (*sine amplitude*)

$$\varphi = \mathrm{am}(u,k), \qquad \zeta = \sin\varphi = \mathrm{sn}(u,k). \tag{20}$$

Two related functions, namely, cn (*cosine amplitude*) and dn (*delta amplitude*), are introduced by the formulas

$$\mathrm{cn}(u,k) = \sqrt{1-\zeta^2} = \cos\varphi, \quad \mathrm{dn}(u,k) = \sqrt{1-k^2\zeta^2} = \sqrt{1-k^2\mathrm{sn}^2(u,k)}. \tag{21}$$

The functions $\mathrm{sn}(u,k)$, $\mathrm{cn}(u,k)$ and $\mathrm{dn}(u,k)$ are called *Jacobian elliptic functions*. Their derivatives with respect to the argument u are obtained directly from the definitions

$$\frac{\mathrm{d}}{\mathrm{d}u}(\mathrm{sn}\,u) = \mathrm{cn}\,u\,\mathrm{dn}\,u, \quad \frac{\mathrm{d}}{\mathrm{d}u}(\mathrm{cn}\,u) = -\mathrm{sn}\,u\,\mathrm{dn}\,u, \quad \frac{\mathrm{d}}{\mathrm{d}u}(\mathrm{dn}\,u) = -k^2\mathrm{sn}\,u\,\mathrm{cn}\,u.$$

Assuming as above the modulus k to be fixed we will simply write $\varphi = \mathrm{am}\,u$, etc. As a consequence of formulas (20) and (21) the following fundamental relations are obtained

$$\mathrm{sn}^2u + \mathrm{cn}^2u = 1, \qquad \mathrm{dn}^2u + k^2\mathrm{sn}^2u = 1, \qquad \mathrm{dn}^2u - k^2\mathrm{cn}^2u = 1 - k^2 \tag{22}$$

and the alternative representations of the elliptic integrals are easily revealed

$$\begin{aligned} F(\varphi,k) \;&=\; F(\mathrm{am}\,u,k) \equiv u = \int_0^u \mathrm{d}\tilde{u} \\ E(\varphi,k) \;&=\; E(\mathrm{am}\,u,k) = \int_0^u \mathrm{dn}^2\tilde{u}\,\mathrm{d}\tilde{u}. \end{aligned} \tag{23}$$

In the case of $\zeta = 1$, respectively $\varphi = \pi/2$, the integrals (18) – (19) are said to be *complete elliptic integrals* of the respective first and second kind

$$K(k) = F(\pi/2,k), \qquad E(k) = E(\pi/2,k). \tag{24}$$

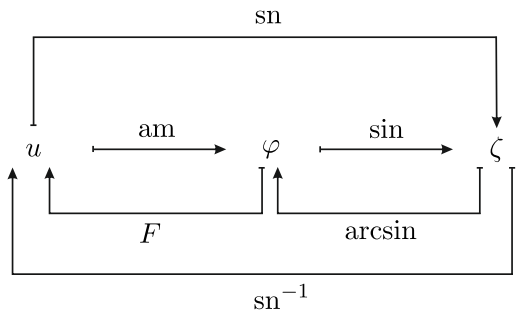

Figure 7. Commutative diagram for the inversion of the normal elliptic integral of the first kind.

In the process of reversing and canonizing the elliptic integrals we find it useful to visualize the composite functions by commutative "barred arrow diagrams" as the one displayed in Fig. 7.

4. Delaunay Shapes of First $\mathcal{D}^{\mathrm{I}}$ and Second Class $\mathcal{D}^{\mathrm{II}}$

As shown above, drop's shapes of the first and the second class $\mathcal{D}^{\mathrm{I}}(\nu)$ and $\mathcal{D}^{\mathrm{II}}(\nu)$ (Fig. 5) are portions of Delaunay surfaces (cf. Fig. 6) lying outside the cylinder $\nu = 0$, whose profile curves (upper right parts), according to equations (12) and (14), are given by the formula

$$z_i(\chi) = \frac{r}{2|\nu+1|}\int_1^{\chi} \frac{((\nu+1)t-\nu+1)\mathrm{d}t}{\sqrt{t(1-t)(t-\sigma_i)}}, \qquad \chi = \frac{x^2}{r^2}, \quad x \in [r, r\sqrt{\sigma_i}] \tag{25}$$

where the root σ_i ($i = 1, 2$) calculated by (16) ($\sigma_i \equiv \bar{\sigma}$) for the surfaces of the respective class

$$\mathcal{D}^{\mathrm{I}}(\nu)\colon\ \nu \in (-\infty, -1) \qquad \text{or} \qquad \mathcal{D}^{\mathrm{II}}(\nu)\colon\ \nu \in (-1, 0) \tag{26}$$

is such that the following inequalities hold (compare with the first and the second item in (17))

$$1 < t < \sigma_i, \qquad 1 \le \chi \le \sigma_i, \qquad i = 1, 2. \tag{27}$$

On substituting with

$$t = 1 + \xi^2, \qquad \chi = 1 + \tilde{\chi}^2, \qquad \xi > 0, \qquad \tilde{\chi} \ge 0$$

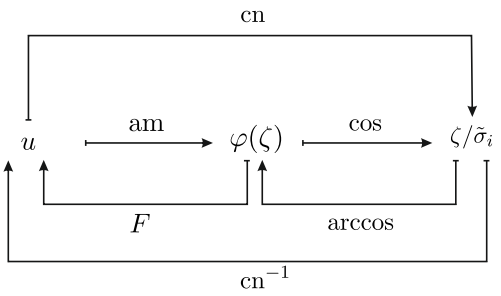

Figure 8. Commutative diagram illustrating the "inversion procedure" for the canonization of the elliptic integral (29).

the polynomial under the radical in (25) is transformed to a product of a sum and a difference of squares

$$z_i(\tilde{\chi}) = \frac{r}{|\nu+1|}\int_0^{\tilde{\chi}} \frac{((\nu+1)\xi^2+2)\mathrm{d}\xi}{\sqrt{(1+\xi^2)(\tilde{\sigma}_i^2-\xi^2)}}, \qquad i=1,2 \tag{28}$$

where

$$\tilde{\sigma}_i = \sqrt{\sigma_i - 1}, \qquad 0<\xi<\tilde{\sigma}_i, \qquad 0\le\tilde{\chi}\le\tilde{\sigma}_i.$$

In this way the integral can be split into two integrals

$$z_i(\tilde{\chi}) = \frac{r}{|\nu+1|}\left(\int_0^{\tilde{\sigma}_i} \frac{((\nu+1)\xi^2+2)\mathrm{d}\xi}{\sqrt{(1+\xi^2)(\tilde{\sigma}_i^2-\xi^2)}} - \int_{\tilde{\chi}}^{\tilde{\sigma}_i} \frac{((\nu+1)\xi^2+2)\mathrm{d}\xi}{\sqrt{(1+\xi^2)(\tilde{\sigma}_i^2-\xi^2)}}\right)$$

each of which is obtained as a special case of the elliptic integral

$$\int_{\zeta}^{\tilde{\sigma}_i} \frac{((\nu+1)\xi^2+2)\mathrm{d}\xi}{\sqrt{(1+\xi^2)(\tilde{\sigma}_i^2-\xi^2)}}, \qquad 0\le\zeta<\tilde{\sigma}_i, \qquad i=1,2 \tag{29}$$

for $\zeta=0$ and $\zeta=\tilde{\chi}$, respectively. The integral (29) can be reduced to its canonical form with the help of the Jacobian cosine elliptic function, replacing ξ and ζ by the new variables $\tilde{u}$ and u

$$\xi = \tilde{\sigma}_i \mathrm{cn}(\tilde{u}, k_i), \quad \zeta = \tilde{\sigma}_i \mathrm{cn}(u, k_i), \quad u = F(\varphi(\zeta), k_i), \quad u\in(0, K(k_i)] \tag{30}$$

thereby employing the "inversion procedure" illustrated by the commutative diagram in Fig. 8 where

$$\varphi := \varphi(\zeta) = \arccos\left(\frac{\zeta}{\tilde{\sigma}_i}\right), \qquad k_i = \frac{\tilde{\sigma}_i}{\sqrt{1+\tilde{\sigma}_i^2}}, \qquad i=1,2. \tag{31}$$

Hence, the reduction of the elliptic integral (29) follows in succession

$$\int\limits_{\zeta}^{\tilde{\sigma}_i}\frac{((\nu+1)\xi^2+2)\mathrm{d}\xi}{\sqrt{(1+\xi^2)(\tilde{\sigma}_i^2-\xi^2)}}=\int\limits_{0}^{u}\frac{((\nu+1)\tilde{\sigma}_i^2\,\mathrm{cn}^2\tilde{u}+2)\mathrm{dn}\,\tilde{u}\,\mathrm{d}\tilde{u}}{\sqrt{1+\tilde{\sigma}_i^2-\tilde{\sigma}_i^2\,\mathrm{sn}^2\tilde{u}}}$$

$$=\frac{1}{\sqrt{1+\tilde{\sigma}_i^2}}\int\limits_{0}^{u}\frac{((\nu+1)\tilde{\sigma}_i^2\,\mathrm{cn}^2\tilde{u}+2)\mathrm{dn}\,\tilde{u}\,\mathrm{d}\tilde{u}}{\sqrt{1-k_i^2\,\mathrm{sn}^2\tilde{u}}}$$

$$=\frac{1}{\sqrt{1+\tilde{\sigma}_i^2}}\Big(2\int\limits_{0}^{u}\mathrm{d}\tilde{u}+(\nu+1)\tilde{\sigma}_i^2\int\limits_{0}^{u}\mathrm{cn}^2\tilde{u}\mathrm{d}\tilde{u}\Big) \tag{32}$$

$$=\frac{1}{\sqrt{1+\tilde{\sigma}_i^2}}\Big(2\int\limits_{0}^{u}\mathrm{d}\tilde{u}+\frac{(\nu+1)\tilde{\sigma}_i^2}{k_i^2}\Big(\int\limits_{0}^{u}\mathrm{dn}^2\tilde{u}\mathrm{d}\tilde{u}-(1-k_i^2)\int\limits_{0}^{u}\mathrm{d}\tilde{u}\Big)\Big)$$

$$=\frac{1}{k_i^2\sqrt{1+\tilde{\sigma}_i^2}}\Big(\big(2k_i^2-(\nu+1)(1-k_i^2)\tilde{\sigma}_i^2\big)F(\varphi,k_i)+(\nu+1)\tilde{\sigma}_i^2E(\varphi,k_i)\Big).$$

In the above chain of equalities we have made use of the fundamental relations (22), the normal elliptic integrals (23) and the formula for the differentiation of the Jacobian cosine function (see above in Section 3). On returning back to the profile curve (28), we make two substitutions in the last line of (32), $\zeta=0$ and $\zeta=\tilde{\chi}$, and then, by subtracting the obtained expressions, we are led to the canonical form (cf. [2, Formula (213.13)])

$$z_i(\tilde{\chi})=\frac{r}{k_i^2\big|\nu+1\big|\sqrt{1+\tilde{\sigma}_i^2}}\Big(\big(2k_i^2-(\nu+1)(1-k_i^2)\tilde{\sigma}_i^2\big)\Big(K(k_i)-F(\varphi(\tilde{\chi}),k_i)\Big)$$

$$+(\nu+1)\tilde{\sigma}_i^2\Big(E(k_i)-E(\varphi(\tilde{\chi}),k_i)\Big)\Big),\quad \tilde{\chi}=\sqrt{\frac{x^2}{r^2}-1},\quad x\in[r,r\sqrt{\sigma_i}]$$

where the complete elliptic integrals $K(k_1)$ and $E(k_1)$ are obtained from the incomplete ones with argument $\varphi(0)=\pi/2$ (cf. equations (24) and (31)).

Written with the help of the variable x the above expression provides explicit parameterizations of the profile curves of the drop's shapes of the first class $\mathcal{D}^{\mathrm{I}}$ and the second one $\mathcal{D}^{\mathrm{II}}$ in Monge representation ($i=\,1,\,2$)

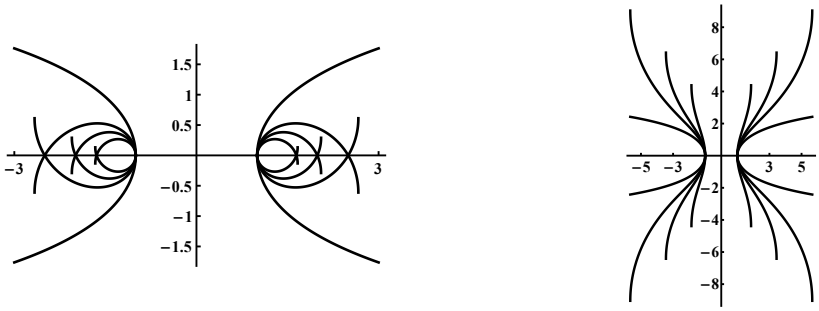

Figure 9. A catenary ($\nu = -1$) with an ensemble of nodaries $\mathcal{D}^{\mathrm{I}}(-2.2)$, $\mathcal{D}^{\mathrm{I}}(-2.9)$ and $\mathcal{D}^{\mathrm{I}}(-4)$ (left) and an ensemble of undularies $\mathcal{D}^{\mathrm{II}}(-0.7)$, $\mathcal{D}^{\mathrm{II}}(-0.55)$ and $\mathcal{D}^{\mathrm{II}}(-0.3)$ (right), both read from outside to inside.

$$z_i(x) = r\Big(K(k_i) - F(\varphi(x), k_i) + \frac{1-\nu}{1+\nu}\big(E(k_i) - E(\varphi(x), k_i)\big)\Big)$$
$$\varphi(x) = \arccos\sqrt{\frac{(x/r)^2 - 1}{\sigma_i - 1}}, \qquad k_i = \frac{2\sqrt{-\nu}}{1-\nu}, \qquad x \in [r, r\sqrt{\sigma_i}] \tag{33}$$

where σ_i is the root $\bar{\sigma}$ calculated by formula (16) for the surfaces in the i-th class. Surfaces described by $z_i(x)$ in (33) are actually portions of Delaunay surfaces – nodoids $\mathcal{D}^{\mathrm{I}}(\nu)$: $\nu \in (-\infty, -1)$ and unduloids $\mathcal{D}^{\mathrm{II}}(\nu)$: $\nu \in (-1, 0)$, obtained respectively for $i = 1$ and $i = 2$.

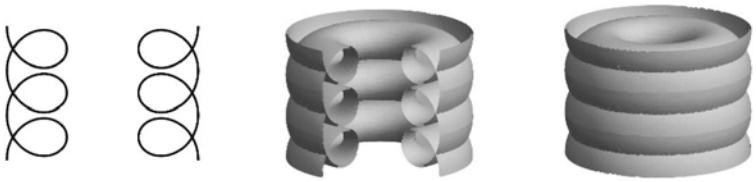

Figure 10. The nodoid $\mathcal{D}^{\mathrm{I}}(-2.2)$ with and without a cut and its profile curve (left).

The above formula describes the upper right part of the profile curve. The whole curve is obtained by two consecutively applied reflections with respect to the coordinate axes OX and OZ (cf. Fig. 2). Graphics of profile curves – two ensembles of three curves each, nodaries $\mathcal{D}^{\mathrm{I}}$ and undularies $\mathcal{D}^{\mathrm{II}}$, are given in Fig. 9.

Figure 11. Ensemble of nodoid shapes with a cut $\mathcal{D}^{\mathrm{I}}(-2.2)$, $\mathcal{D}^{\mathrm{I}}(-2.9)$ and $\mathcal{D}^{\mathrm{I}}(-4)$ (from outside to inside) and their profile curves (left).

The next two canonical representations of the surfaces of classes $\mathcal{D}^{\mathrm{I}}$ and $\mathcal{D}^{\mathrm{II}}$ are obtained from (33) by introducing two real parameters. One of these parameters $v \in [0, 2\pi]$ measures the angular coordinate of the meridians while the other parameter u is related to $\tilde{\chi}$ (respectively to the coordinate x) in two different ways, either by the equations

$$u = \operatorname{arccsc}\sqrt{1+\tilde{\chi}^2} = \operatorname{arccsc}\left(\frac{x}{r}\right), \qquad u \in \left[\operatorname{arccsc}\sqrt{\sigma_i},\ \frac{\pi}{2}\right] \tag{34}$$

or by the equations

$$u = \operatorname{cn}^{-1}\Big(\frac{\tilde{\chi}}{\tilde{\sigma}_i}\Big) = \operatorname{cn}^{-1}\Big(\sqrt{\frac{(x/r)^2-1}{\sigma_i-1}}\Big), \qquad u\in[0,\ 2K(k_i)]\,. \tag{35}$$

The corresponding canonical representations of the drop's shapes – the nodoids $\mathcal{D}^{\mathrm{I}}(\nu)$: $\nu \in (-\infty, -1)$ and the unduloids $\mathcal{D}^{\mathrm{II}}(\nu)$: $\nu \in (-1, 0)$ are given either by the set of equations

$$\begin{aligned} z_i(u) &= r\Big(K(k_i) - F(\varphi(u), k_i) + \frac{1-\nu}{1+\nu}\big(E(k_i) - E(\varphi(u), k_i)\big)\Big) \\ \varphi(u) &= \operatorname{arccos}\Big(\frac{\cot u}{\sqrt{\sigma_i - 1}}\Big), \qquad \beta = \operatorname{arccsc}\sqrt{\sigma_i} \\ x(u,v) &= r\csc u\,\cos v, \quad y(u,v) = r\csc u\,\sin v, \quad z(u,v) = z_i(u), \quad u \in \Big[\beta,\ \frac{\pi}{2}\Big]\,. \end{aligned} \tag{36}$$

Alternatively, they can be described by another set of formulas in which appears the same parameter u (running however in a different interval) and the same axial variable $v \in [0, 2\pi]$, i.e.,

$$\begin{aligned} x_i(u) &= r\sqrt{\sigma_i}\,\operatorname{dn} u, \qquad u \in [0,\ 2K(k_i)]\,, \qquad v \in [0, 2\pi] \\ z_i(u) &= r\Big(K(k_i) - u + \frac{1-\nu}{1+\nu}\big(E(k_i) - E(\operatorname{am} u, k_i)\big)\Big) \\ x(u,v) &= x_i(u)\cos v, \qquad y(u,v) = x_i(u)\sin v, \qquad z(u,v) = z_i(u) \end{aligned} \tag{37}$$

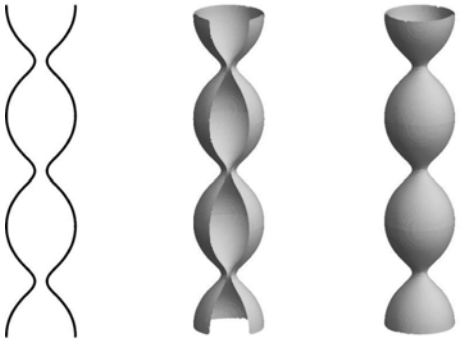

Figure 12. The unduloid $\mathcal{D}^{\mathrm{II}}(-0.7)$ with and without a cut and its profile curve (left).

where k_i (for i = 1 and i = 2) is defined in (33). Using one and the same notation u for parameters with different meanings and different ranges allows different parameterizations to be represented uniformly and this generally does not lead to confusion. Nevertheless one must be careful not to confuse the parameter u in the representation (34) with the variable u that has been previously used for denoting the values of the normal elliptic integral of the first kind (cf. the definitions (23)).

In the same time the variable u in the representation (35) appears in exactly that previous meaning, related here with the inverse of the Jacobian cosine function. The latter becomes at once transparent if one looks at the commutative diagram in Fig. 8 with the variable ζ replaced by $\tilde{\chi}$. Various drop's shapes of the first and the second class are given in Fig. 10 – Fig. 13. Note also that when $\nu \to -\infty$ the surfaces degenerate to a circle with radius r.

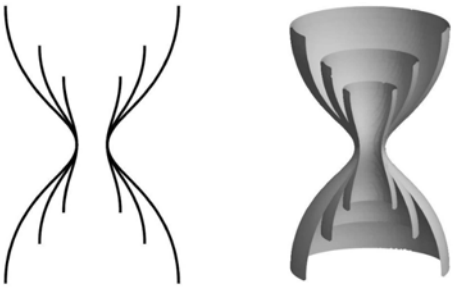

Figure 13. Ensemble of unduloid shapes with a cut $\mathcal{D}^{\mathrm{II}}(-0.3)$, $\mathcal{D}^{\mathrm{II}}(-0.55)$ and $\mathcal{D}^{\mathrm{II}}(-0.7)$ (from inside to outside) and their profile curves (left).

5. Delaunay Shapes of Third $\mathcal{D}^{\mathrm{III}}$ and Fourth Class $\mathcal{D}^{\mathrm{IV}}$

Drop's shapes of the third $\mathcal{D}^{\mathrm{III}}(\nu)$ and the fourth class $\mathcal{D}^{\mathrm{IV}}(\nu)$ (Fig. 5) are portions of Delaunay surfaces, unduloids and nodoids respectively (cf. Fig. 6), lying inside the cylinder $\nu = 0$. According to equations (12) – (13) their profile curves (upper right parts) are given by the formula

$$z_i(\chi) = \frac{r}{2(\nu+1)} \int_{\chi}^{1} \frac{((\nu+1)t - \nu + 1)\mathrm{d}t}{\sqrt{t(1-t)(t-\sigma_i)}}, \quad \chi = \frac{x^2}{r^2}, \qquad x \in [r\sqrt{\sigma_i}, r] \tag{38}$$

where the root σ_i ($i = 3,\, 4$) calculated by (16) ($\sigma_i \equiv \bar{\sigma}$) for the surfaces of the respective class

$$\mathcal{D}^{\mathrm{III}}(\nu)\colon\ \nu \in (0,1) \qquad \text{or} \qquad \mathcal{D}^{\mathrm{IV}}(\nu)\colon\ \nu \in (1,\infty) \tag{39}$$

is such that the following inequalities hold (compare with the third and the forth item in (17))

$$0 < \sigma_i < t < 1, \qquad 0 < \sigma_i \le \chi \le 1, \qquad i = 3, 4. \tag{40}$$

The reduction of the above elliptic integral goes through the "inversion procedure",

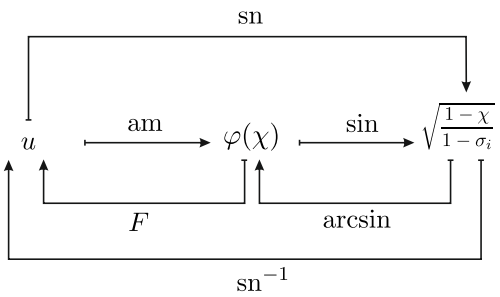

Figure 14. Commutative diagram illustrating the "inversion procedure" for the canonization of the elliptic integral (38).

as illustrated by the commutative diagram in Fig. 14, on writing

$$\begin{aligned} t &= 1 - (1-\sigma_i)\mathrm{sn}^2(\tilde{u}, k_i) \equiv \mathrm{dn}^2(\tilde{u}, k_i) \\ \chi &= 1 - (1-\sigma_i)\mathrm{sn}^2(u, k_i) \equiv \mathrm{dn}^2(u, k_i) \end{aligned} \tag{41}$$

where

$$u = F(\varphi(\chi), k_i), \qquad \varphi(\chi) = \arcsin\sqrt{\frac{1-\chi}{1-\sigma_i}}, \qquad k_i = \sqrt{1-\sigma_i}\,. \tag{42}$$

By substituting and integrating in succession the profile curve in (38) is reduced to a representation involving only normal elliptic integrals of the first and the second kind (cf. [2, Formula (236.16)])

$$\begin{aligned} z_i(\chi) &= \frac{r}{\nu+1}\int_0^u \frac{\big(2-(\nu+1)(1-\sigma_i)\mathrm{sn}^2\tilde{u}\big)\,\mathrm{dn}\,\tilde{u}\,\mathrm{d}\tilde{u}}{\sqrt{1-(1-\sigma_i)\mathrm{sn}^2\tilde{u}}} \\ &= \frac{r}{\nu+1}\int_0^u \frac{\big(2-(\nu+1)(1-\sigma_i)\mathrm{sn}^2\tilde{u}\big)\,\mathrm{dn}\,\tilde{u}\,\mathrm{d}\tilde{u}}{\sqrt{1-k_i^2\,\mathrm{sn}^2\tilde{u}}} \\ &= r\int_0^u \left(\frac{2}{\nu+1} - (1-\sigma_i)\mathrm{sn}^2\tilde{u}\right)\mathrm{d}\tilde{u} \\ &= r\left(\frac{2}{\nu+1}\int_0^u \mathrm{d}\tilde{u} - \frac{1-\sigma_i}{k_i^2}\Big(\int_0^u \mathrm{d}\tilde{u} - \int_0^u \mathrm{dn}^2\tilde{u}\,\mathrm{d}\tilde{u}\Big)\right) \\ &= r\left(\frac{1-\nu}{1+\nu}\,F(\varphi(\chi),k_i) + E(\varphi(\chi),k_i)\right). \end{aligned} \tag{43}$$

In the above chain of equalities we have made use of the formulas (20) – (23) and the formula for the derivative of the Jacobian sine elliptic function (cf. Section 3).

On returning back to the variable x in the last line of (43) we arrive at our first explicit parameterization of the profile curves of the drop's shapes of the third $\mathcal{D}^{\mathrm{III}}$ and the fourth class $\mathcal{D}^{\mathrm{IV}}$ in Monge representation

$$\begin{aligned} z_i(x) &= r\Big(\frac{1-\nu}{1+\nu}\,F(\varphi(x),k_i) + E(\varphi(x),k_i)\Big), \qquad i=3,4 \\ \varphi(x) &= \arcsin\Big(\frac{\sqrt{1-(x/r)^2}}{k_i}\Big), \qquad k_i = \frac{2\sqrt{\nu}}{1+\nu}, \qquad x\in[r\sqrt{\sigma_i}, r]. \end{aligned} \tag{44}$$

Here σ_i is the root $\bar{\sigma}$ calculated by formula (16) for the surfaces of the respective i-th class. Each one of the surfaces in the two classes $\mathcal{D}^{\mathrm{III}}$ and $\mathcal{D}^{\mathrm{IV}}$, which profile

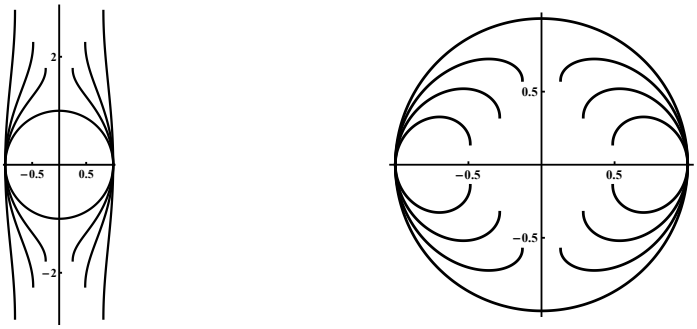

Figure 15. A circle ($\nu = 1$) with an ensemble of undularies $\mathcal{D}^{\mathrm{III}}(0.1)$, $\mathcal{D}^{\mathrm{III}}(0.35)$ and $\mathcal{D}^{\mathrm{III}}(0.6)$ (left) and an ensemble of nodaries $\mathcal{D}^{\mathrm{IV}}(1.3)$, $\mathcal{D}^{\mathrm{IV}}(1.8)$ and $\mathcal{D}^{\mathrm{IV}}(2.9)$ (right), both read from outside to inside.

curve is given by (44) for $i = 3, 4$, is a particular portion of a Delaunay surface, being either a unduloid $\mathcal{D}^{\mathrm{III}}(\nu)$ for some $\nu \in (0, 1)$, or a nodoid $\mathcal{D}^{\mathrm{IV}}(\nu)$ for some $\nu \in (1, \infty)$.

Note that the above formula describes only the upper right part of the profile curve. The whole curve is obtained by performing two consecutively reflections with respect to the coordinate axes OX and OZ (cf. Fig. 2). Graphics of the profile curves obtained in this way are combined in two ensembles by three undularies $\mathcal{D}^{\mathrm{III}}$ and three nodaries $\mathcal{D}^{\mathrm{IV}}$ are presented in Fig. 15.

Now we are going to give two canonical representations of the surfaces of the third and fourth classes obtained from (44) by substituting for χ (respectively the coordinate x) the parameter u, defined in two different ways, either by the equations

$$u = \arcsin\sqrt{\chi} = \arcsin\left(\frac{x}{r}\right), \qquad u \in \left[\arcsin\sqrt{\sigma_i},\ \frac{\pi}{2}\right] \tag{45}$$

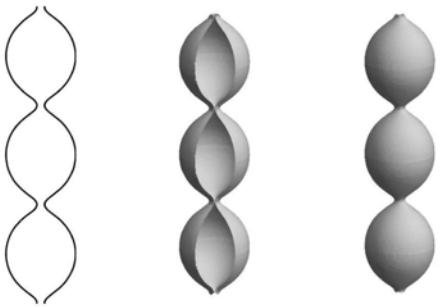

Figure 16. The unduloid $\mathcal{D}^{\mathrm{III}}(0.8)$ with and without a cut and its profile curve (left).

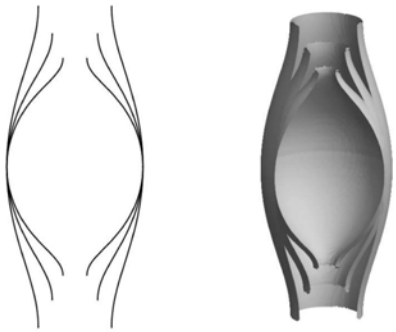

Figure 17. Ensemble of unduloid shapes with a cut $\mathcal{D}^{\mathrm{III}}(0.3)$, $\mathcal{D}^{\mathrm{III}}(0.5)$ and $\mathcal{D}^{\mathrm{III}}(0.7)$ (from outside to inside) and their profile curves (left).

or by the equations

$$u = \mathrm{sn}^{-1}\Big(\sqrt{\frac{1-\chi}{1-\sigma_i}}\Big) = \mathrm{dn}^{-1}\Big(\frac{x}{r}\Big), \qquad u\in[-K(k_i),\, K(k_i)]\,. \tag{46}$$

We have two choices for the parameter u, fixed by the equations (45) and (46), and they have different ranges and different relationships with the variable χ (respectively x). This however should not create confusion in the respective parameterizations of the surfaces and their profile curves. The commutative diagram in Fig. 14 may serve to clarify the meaning of the second choice. As a result the corresponding canonical representations of the drop's shapes – the unduloids $\mathcal{D}^{\mathrm{III}}(\nu)$: $\nu \in (0,1)$ and the nodoids $\mathcal{D}^{\mathrm{IV}}(\nu)$: $\nu \in (1,\infty)$, are given for $i = 3, 4$, respectively, either by the set of equations

$$\begin{aligned} z_i(u) &= r\Big(\frac{1-\nu}{1+\nu}\,F(\varphi(u),k_i) + E(\varphi(u),k_i)\Big) \\ \varphi(u) &= \arcsin\Big(\frac{\cos u}{k_i}\Big), \qquad \beta = \arcsin\sqrt{\sigma_i} \end{aligned} \tag{47}$$

$$x(u,v) = r\sin u\,\cos v, \quad y(u,v) = r\sin u\,\sin v, \quad z(u,v) = z_i(u), \quad u \in \Big[\beta, \frac{\pi}{2}\Big]$$

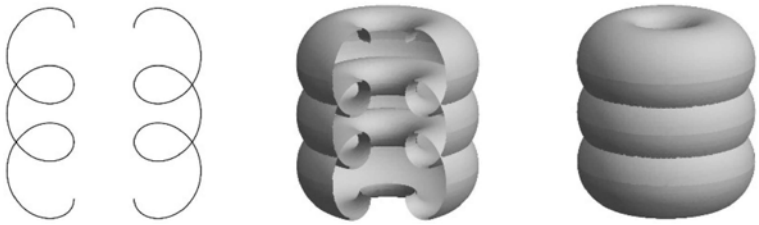

Figure 18. The nodoid $\mathcal{D}^{\mathrm{IV}}(1.9)$ with and without a cut and its profile curve (left).

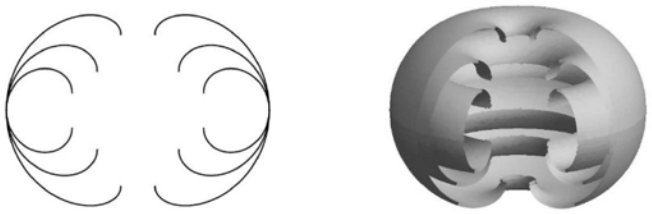

Figure 19. Ensemble of nodoid shapes with a cut $\mathcal{D}^{\mathrm{IV}}(1.3)$, $\mathcal{D}^{\mathrm{IV}}(1.9)$ and $\mathcal{D}^{\mathrm{IV}}(3)$ (from outside to inside) and their profile curves (left).

or by another set of equations in which the parameter u appears again, but this time in a different range, i.e.,

$$\begin{aligned} x_i(u) &= r\,\mathrm{dn}\,u, \qquad u \in [-K(k_i),\, K(k_i)]\,, \qquad v \in [0, 2\,\pi] \\ z_i(u) &= r\Big(\frac{1-\nu}{1+\nu}\,u + E(\mathrm{am}\,u, k_i)\Big) \\ x(u,v) &= x_i(u)\cos v, \qquad y(u,v) = x_i(u)\sin v, \qquad z(u,v) = z_i(u). \end{aligned} \tag{48}$$

The respective moduli k_i are defined in (44). Notice that the second parameter v, which is the same for both parameterizations, coincides with the angular coordinate of the meridians.

Various drop's shapes of the third and the fourth class are given in Fig. 16 – Fig. 19. Notice also that when $\nu \to \infty$ these surfaces degenerate to a circle with radius r.

6. Concluding Remarks

At the mid 1850s Joseph Plateau (a Belgiian physicists) carried out the first systematic studies of the rotating liquid drops as a part of his famous surface tension experiments [18]. Curiously enough it was approximately at the time when Charles-Eugène Delaunay (a French mathematician) had classified in 1841 all surfaces of revolution with a constant mean curvature [4]. These axially symmetric surfaces were later called Delaunay's surfaces. As we have shown above, there exists an interesting connection between the rotating liquid drops of Plateau and Delaunay's surfaces. Under certain conditions a drop, held together by the action of surface tension and rotating uniformly, assumes the shape of a Delaunay surface. This happens when the mass densities of the liquid drop itself, ρ_i, and of the fluid that fills the surrounding space, ρ_e, are equal to each other: $\rho \equiv \rho_i - \rho_e = 0$. By introducing two pure geometric parameters, one of which, r, is measuring the size and the other, ν, is accounting for the shape of the Delaunay surfaces, we have distinguished four particular classes of the drop's shape, being either portions of

Table 1. Various relationships referring to the curvatures, κ_π, κ_μ and H, and the pressure difference p, for different types of Delaunay shapes of the rotating liquid drop.

Delaunay Surfaces	Principal Curvatures	Mean Curvature	Pressure Difference
nodoids $\mathcal{D}^{\mathrm{I}}(\nu)$ $\nu < -1$	$\kappa_\mu < \kappa_\pi,\ \kappa_\mu < 0$	$H < 0$	$p < 0$
catenoids $\nu = -1$	$\kappa_\mu = -\kappa_\pi < 0$	$H = 0$	$p = 0$
unduloids $\mathcal{D}^{\mathrm{II}}(\nu)$ $\nu \in (-1, 0)$	$\kappa_\mu < \kappa_\pi,\ \kappa_\pi > 0$	$H > 0$	$p > 0$
cylinders $\nu = 0$	$\kappa_\mu = 0,\ \kappa_\pi = \frac{1}{r}$	$H = \frac{1}{2r}$	$p = \frac{\sigma}{2r}$
unduloids $\mathcal{D}^{\mathrm{III}}(\nu)$ $\nu \in (0, 1)$	$\kappa_\mu < \kappa_\pi,\ \kappa_\pi > 0$	$H > 0$	$p > 0$
spheres $\nu = 1$	$\kappa_\mu = \kappa_\pi = \frac{1}{r}$	$H = \frac{1}{r}$	$p = \frac{\sigma}{r}$
nodoids $\mathcal{D}^{\mathrm{IV}}(\nu)$ $\nu > 1$	$\kappa_\mu > \kappa_\pi,\ \kappa_\mu > 0$	$H > \frac{1}{r}$	$p > \frac{\sigma}{r}$

nodoids of class $\mathcal{D}^{\mathrm{I}}(\nu)$, for $\nu < -1$, and class $\mathcal{D}^{\mathrm{IV}}(\nu)$, for $\nu > 1$, or portions of unduloids of classes $\mathcal{D}^{\mathrm{II}}(\nu)$ and $\mathcal{D}^{\mathrm{III}}(\nu)$, for $\nu \in (-1, 0)$ and $\nu \in (0, 1)$, respectively (cf. the classification (17) and Fig. 6). The rest of the Delaunay surfaces (excluding the plane) have been classified as follows: catenoids $\nu = -1$, right circular cylinders $\nu = 0$, and spheres $\nu = 1$.

By making use of the canonical forms of the elliptic integrals and the Jacobian elliptic functions, we have obtained several explicit parameterizations of the unduloids and nodoids, which, as it is well known, are surfaces that do not have closed

form description in elementary functions. Thus we have parameterized all the Delaunay shapes of the rotating liquid drops, namely, we have described explicitly a two parametric family of CMC axially symmetric surfaces, which mean curvature as a function of the two characteristic parameters r and ν is given by

$$H = \frac{1+\nu}{2r}.$$

Besides, we have established that the principal curvatures of these surfaces expressed as functions of the distance $\mathcal{R}$ from the axis of revolution have the form

$$\kappa_\pi = \frac{1+\nu}{2r} + \frac{(1-\nu)r}{2\mathcal{R}^2}, \qquad \kappa_\mu = \frac{1+\nu}{2r} - \frac{(1-\nu)r}{2\mathcal{R}^2} \tag{49}$$

where $\mathcal{R}$ is within the interval $[r,\ r\sqrt{\overline{\sigma}}]$ for the surfaces of classes $\mathcal{D}^{\mathrm{I}}$ and $\mathcal{D}^{\mathrm{II}}$ or belongs to the interval $[r\sqrt{\overline{\sigma}},\ r]$ for classes $\mathcal{D}^{\mathrm{III}}$ and $\mathcal{D}^{\mathrm{IV}}$ (cf. equations (8) and (11)). As it follows from these equations the ratio between the pressure difference p and the surface tension σ can be expressed through the geometric parameters r and ν

$$p = \frac{(1+\nu)\sigma}{2r}.$$

Based on the above formulae we have related in Table 1 the principal curvatures κ_π and κ_μ for each one of the four classes of surfaces, and as well as, returning back to the physical conditions, we have compared the values (and particularly the signs) of the mean curvature H and the pressure difference p with respect to their dependencies on r and ν. The significance of these relationships can be understood in connection with some other framework – the capillary action and wetting phenomena. As can be seen from the above equations and the last two columns of Table 1, the pressure difference $p = p_i - p_e$ changes its value and sign in accordance with the Laplace-Young equation (1) which is a direct consequence of the pressure balance equation (2) in the case of equal mass densities, i.e., $\rho \equiv 0$.
In this regard it is worth noting that for a narrower interval $\mathcal{R} \in [r,\ r\sqrt[4]{\overline{\sigma}}]$ the nodoids of class $\mathcal{D}^{\mathrm{I}}$ can be referred as *anticlastic surfaces* (having opposite signs of their principal curvatures), while the nodoids of class $\mathcal{D}^{\mathrm{IV}}$, if considered for $\mathcal{R} \in [r\sqrt[4]{\overline{\sigma}},\ r]$, belong to the *synclastic type of surfaces* (with the same signs of the principal curvatures). A similar classification can also be made for the unduloids of class $\mathcal{D}^{\mathrm{II}}$ and class $\mathcal{D}^{\mathrm{III}}$. This kind of observations concerning the specific relations between the principal curvatures κ_π and κ_μ, which in our considerations are given by (49), is basically connected with the ability of the respective shapes, being here nodoids or unduloids, to form capillary surfaces embracing the liquid drops in case of their contact with solids. More details on how the geometry of the

contact surfaces and the wettability of the solid materials are related with the shape of the capillary surfaces can be found in [7].

References

[1] Athanassenas M., *A Variational Problem for Constant Mean Curvature Surfaces with Free Boundary*, J. Reine Angew. Math. **377** (1987) 97-107.

[2] Byrd P. and Friedman M., *Handbook of Elliptic Integrals for Engineers and Scientists*, 2nd Edn, Springer, New York 1971.

[3] Chandrasekhar S., *The Stability of a Rotating Liquid Drop*, Proc. R. Soc. Lond. A **286** (1965) 1-26.

[4] Delaunay C., *Sur la surface de revolution dont la courbure moyenne est constante*, J. Math. Pures et Appliquées **6** (1841) 309-320.

[5] Gulliver R., *Tori of Prescribed Mean Curvature and the Rotating Drop*, Astérisque **118** (1984) 167-179.

[6] Hadzhilazova M., Mladenov I. and Oprea J., *Unduloids and Their Geometry*, Arch. Mathematicum **43** (2007) 417-429.

[7] Haynes J., *Capillary Equilibrium and Stability in Liquids Under Microgravity*, Bull. Mater. Sci. **4** (1982) 85-102.

[8] López R., *Stationary Rotating Surfaces in Euclidean Space*, Calc. Var. **39** (2010) 333-359.

[9] Mladenov I., *Delaunay Surfaces Revisited*, C. R. Bulg. Acad. Sci. **55** (2002) 19-24.

[10] Mladenov I., *New Solutions of the Shape Equation*, Eur. Phys. J. B **29** (2002) 327-330.

[11] Mladenov I. and Hadzhilazova M., *The Many Faces of Elastica*, Springer, Cham 2017.

[12] Mladenov I. and Oprea J., *On the Geometry of the Rotating Liquid Drop*, Math. Comput. Stimulat. **127** (2016) 194-202.

[13] Nurse A., Coriell S. and McFadden G., *On the Stability of Rotating Drops*, J. Res. Natl. Inst. Stand. Technol. **120** (2015) 74-101

[14] Oprea J., *The Mathematics of Soap Films*: *Exploration with Maple*, American Mathematical Society, Providence 2000.

[15] Oprea J., *Differential Geometry and Its Applications*, 2nd Edn, Prentice Hall, Upper Saddle River 2003.

[16] Palmer B. and Perdomo O., *Equilibrium Shapes of Cylindrical Rotating Liquid Drops*, Bull. Braz. Math. Soc. **46** (2015) 515-561.

[17] Pámpano A., *Planar p-Elasticae and Rotational Linear Weingarten Surfaces*, Geom. Integrability & Quantization **20** (2019) 227-238.

[18] Plateau J., *Experimental and Theoretical Researches on the Figures of Equilibrium of a Liquid Mass Withdrawn From the Action of Gravity*, Phil. Mag. **14** (1857) 1-22.

[19] Pulov V., Hadzhilazova M. and Mladenov I., *Delaunay Surfaces in Terms of Weierstrassian Functions*, In: International Conference on Integrability, Recursion Operators and Soliton Interactions, B. Aneva, G. Grahovski, R. Ivanov and D. Mladenov (Eds), Avangard Prima, Sofia 2014, pp 218-224.

[20] Pulov V. and Mladenov I., *Some Classes of Shapes of the Rotating Liquid Drop*, J. Geom. Symmetry Phys. **52** (2019) 67-102.

[21] Radoev B., Petkov P. and Ivanov I., *Capillary Bridges – A Tool for Three-Phase Contact Investigation*, In: Surface Energy, IntechOpen 2015, 32pp.

[22] Rayleigh J., *The Equilibrium of Revolving Liquid Under Capillary Force*, Phil. Mag. **28** (1914) 161-170.

Vladimir I. Pulov
Department of Mathematics and Physics
Technical University of Varna
Varna 9010, BULGARIA
E-mail address: vpulov@hotmail.com

Ivaïlo M. Mladenov
Institute of Biophysics
Bulgarian Academy of Sciences
Acad. G. Bonchev Str., Bl. 21
1113 Sofia, BULGARIA
E-mail address: mladenov@bio21.bas.bg